Development of a Plasma Diagnostics System Using an Impulse Waveform Voltage

Tokihiko TOKUZAWA, Kazuo KAWAHATA, Yasuhiko ITO, Kenji TANAKA, Ichihiro YAMADA and LHD Experimental Group

National Institute for Fusion Science, Toki 509-5292, Japan

(Received 30 November 2007 / Accepted 7 March 2008)

A new application using an electric impulse signal has been developed for electron density profile measurements in the Large Helical Device (LHD). Using an impulse waveform voltage, which has broadband frequency components, we constructed an ultrashort pulsed radar reflectometer with 28 channels in X-, Ka-, and U-band frequency components. The effect of the bandwidth of an inline band-pass filter was investigated, and was optimized. For a multiple-channel and multiple-frequency band system, a new switching technique and multiplexer were developed. Using the Abel inversion method, the reconstructed electron density profile was obtained from the delay time as a function of the probing frequency. Good agreement with other diagnostics was obtained.

Keywords: impulse, microwave radar, electron density profile, microwave reflectometer, LHD

DOI: 10.1585/pfr.3.018

1. Introduction

An impulse waveform voltage can be utilized for electron density profile measurements in high-temperature plasma, because it has broad band frequency components in Fourier space. This means that one electric impulse signal can replace a broadband microwave source. For example, when we use a 10-ps full-width half-maximum (FWHM) impulse, frequency components up to 100 GHz are produced. This impulse is used for producing a pulsed radar for plasma density measurements, which is known as an ultrashort pulsed radar reflectometer [1–3]. Because the radar measurement is conducted over a very short period of time, the plasma can be treated as a stationary object. This means that the effect of fluctuations in the cut-off layer in one frequency scanning period can be ignored. In addition, this ultrashort pulsed radar reflectometer system uses a time-of-flight (TOF) measurement technique. The TOF measurements have the advantage that the ordinary and extraordinary polarization of each component in the reflected wave are distinguishable by the time lag.

In the Large Helical Device (LHD) [4], we developed ultrashort pulsed radar reflectometer systems using two impulse generators. One source was a Picosecond Pulse Labs, Model 4015C Impulse Generator with a Model 5208 Impulse Forming Network, which generates a voltage impulse with an amplitude of −2.2 V and FWHM of 23 ps. The other source was a Model 4016 Impulse Generator with a Model 5206 Impulse Forming Network, which generates an impulse with and an amplitude of −2.0 V amplitude and FWHM of 18 ps. These impulse waveforms and frequency spectra are shown in Fig. 1. Initially, we constructed a six-channel Ka-band (26-40 GHz) microwave reflectometer using a 23-ps impulse [5]. Then, for more detailed and wider-ranging profile measurements, the system was upgraded with the addition of multiple spatial channels and frequency bands.

In Sec. 2 of this paper, we describe the current ultrashort pulsed radar reflectometer system in the LHD, and the experimental procedure for estimating a suitable bandwidth for the inline band-pass filter (BPF). For the system consisting of multiple channels and bands, the new switching technique and multiplexer are presented in Sec. 3. The resultant density profile measured using this reflectometer and the comparison with other diagnostic results are described in Sec. 4. We summarize the results in Sec. 5.

2. Ultrashort Pulsed Radar Reflectometer System

The schematic of the ultrashort pulsed radar reflectometer system is shown in Fig. 2. A Model 4016 Impulse Generator with an amplitude of −2.0 V and FWHM of 18 ps is utilized as an initial source. For obtaining the desired frequency components from this impulse, we utilize the standard rectangular waveguide. When the impulse is launched into the waveguide, it is transformed into a chirped wave that includes broad frequency components of the standard base band. This is caused by the dispersion of electromagnetic wave in the waveguide. The group velocity v_g in the waveguide is described by

$$v_g = c\sqrt{1-(\lambda/2a)^2}. \quad (1)$$

Here, c is the speed of light, a is the long side length of the rectangular waveguide, and λ is the wavelength of the

author's e-mail: tokuzawa@nifs.ac.jp

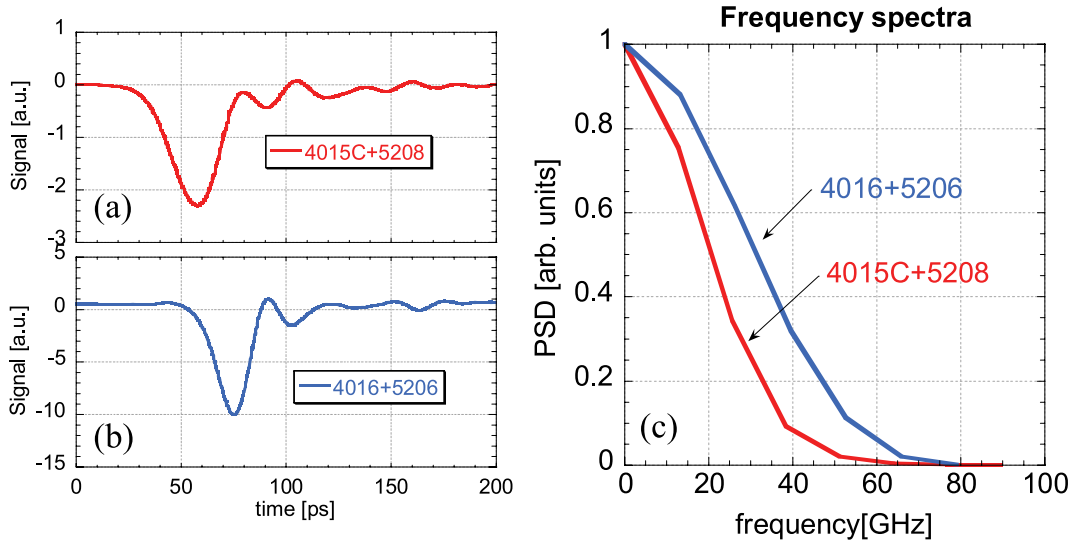

Fig. 1 Waveform of an impulse from (a) PSPL-4015C (FWHM:23 ps) and (b) PSPL-4016 (FWHM:18 ps), and (c) those frequency spectra.

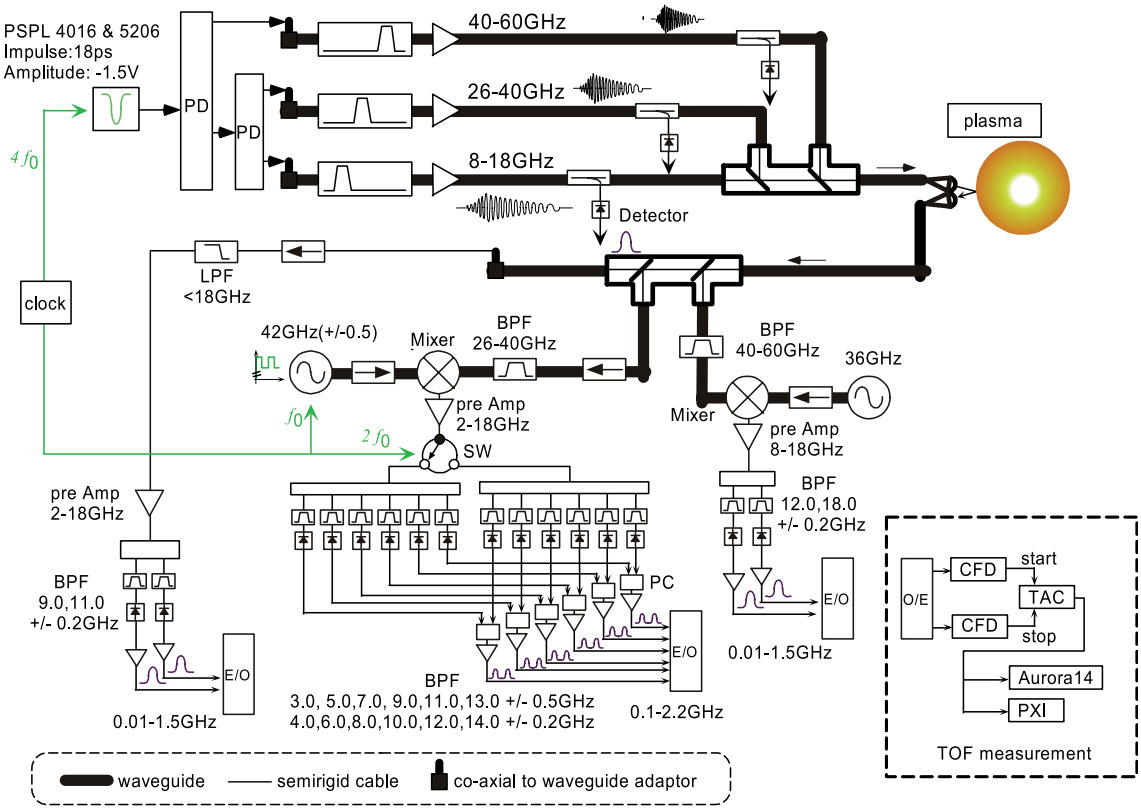

Fig. 2 Schematic view of ultrashort pulsed radar reflectometer system. PD is a power divider, PC is a power combiner, and SW is a single-pole double-throw switch.

electromagnetic wave in vacuum. The chirped wave output from the waveguide is shown in Figs. 3 (a-c), and the resultant frequency components are shown in Figs. 3 (d-f). Here, the frequency is analyzed using the zero-crossing method. The frequency component gradually decreases, and is almost in agreement with the value calculated using Eq. (1). The lowest frequency component is determined by the cut-off frequency of the waveguide. The low-pass filter also filters out frequency components higher than the maximum frequency in the standard frequency band. Therefore, we can obtain a microwave in each desired frequency band. At present, the system has three frequency bands: X-

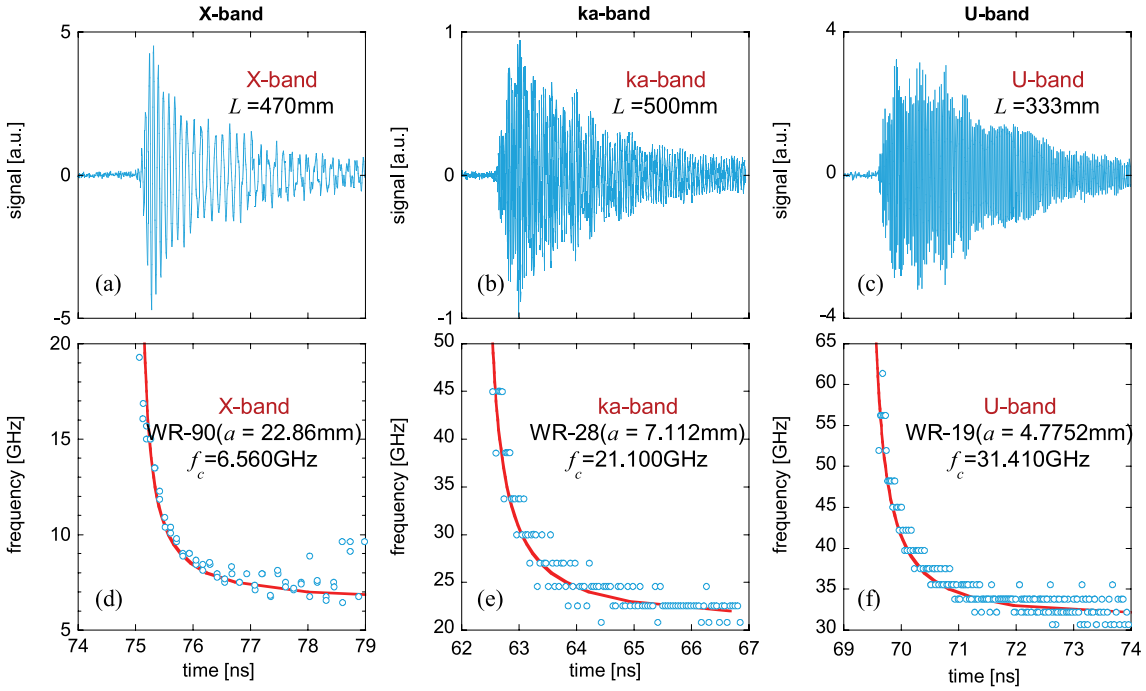

Fig. 3 (a-c) Chirped waveform through each standard rectangular waveguide. (d-f) Temporal evolution of frequency components of each chirped signal (open circles) and calculated values (line). (a, d) X-mode, (b, e) Ka-band, (c, f) U-band.

band, Ka-band, and U-band. Each frequency component is amplified by a corresponding microwave power amplifier, and combined to one transmission line.

The combined chirped microwave is launched into the plasma. The incident wave reflects back from the cut-off layers corresponding to each frequency component. The reflected wave is divided and directed to the detection stage of each frequency band. The X-band frequency components are detected directly through two band-pass filters of 9 and 11 GHz. The Ka-band and U-band components are detected by a super heterodyne detection system. In the mixer, the reflected wave is downshifted by the frequency of a local microwave oscillator. The oscillator frequencies for the Ka-band and U-band components are approximately 42 and 36 GHz, respectively. For the Ka-band, the output from the mixer is amplified by an intermediate frequency (IF) amplifier, and then led to a single-pole double-throw (SPDT) switch. Each IF signal is filtered by 12 BPFs, whose center frequencies range from 3 to 14 GHz. Twelve signals are detected by Schottky-barrier diode detectors to obtain the reflected signal pulses. For the U-band, two BPFs with center frequencies of 12 and 18 GHz are utilized.

The detected pulses are amplified by pulse amplifiers and led to electro-optical (E/O) converters, after which the TOF measurement is conducted. For discriminating the reflected pulse, we utilize constant fraction discriminators (CFD) because the pulse amplitude changes during the plasma discharge. A fraction of the incident wave is extracted using a directional coupler, its power is measured, and this wave is used as a reference pulse. Both the reference pulse as the start signal and the reflected pulse as the stop signal are led to a time-to-amplitude converter (TAC). The output voltage of the TAC is proportional to the time difference between the start and the stop signals. The spatial precision estimated from the TAC output was previously tested, and was found to be less than 6 mm [6].

Figure 4 shows the cross section of the LHD and the transmission path in the vacuum vessel. The transmission line comprises two corrugated waveguides to avoid transmission losses. At the tip of the waveguide, a mirror is attached and used as a launcher towards the plasma center. Since this launcher is located around a groove in the helical coil, the microwave is launched from the high-magnetic field side. The reflected wave is received by another corrugated waveguide using a mirror. These waveguides are wrapped in a carbon sheath to protect them from heat damage, since the waveguides cross the diverter leg region.

One of the benefits of TOF measurement is that data acquisition requirements are small. The acquired signal is the TAC output voltage of each reflected pulse. The required sampling rate is simply the pulse repetition rate. The highest repetition rate is limited by the CFD to 400 kHz. The data is recorded using a Jorway Aurora 14 transient recorder with 1 Mword/ch memory, and the sampling rate is usually set to 100 kHz. Since a real-time data acquisition system was recently developed in the LHD, a sampling rate of up to 10 Msample/sec is possible [7], allowing us to measure during the entire plasma discharge. Figure 5 shows the TOF signals throughout a steady-state

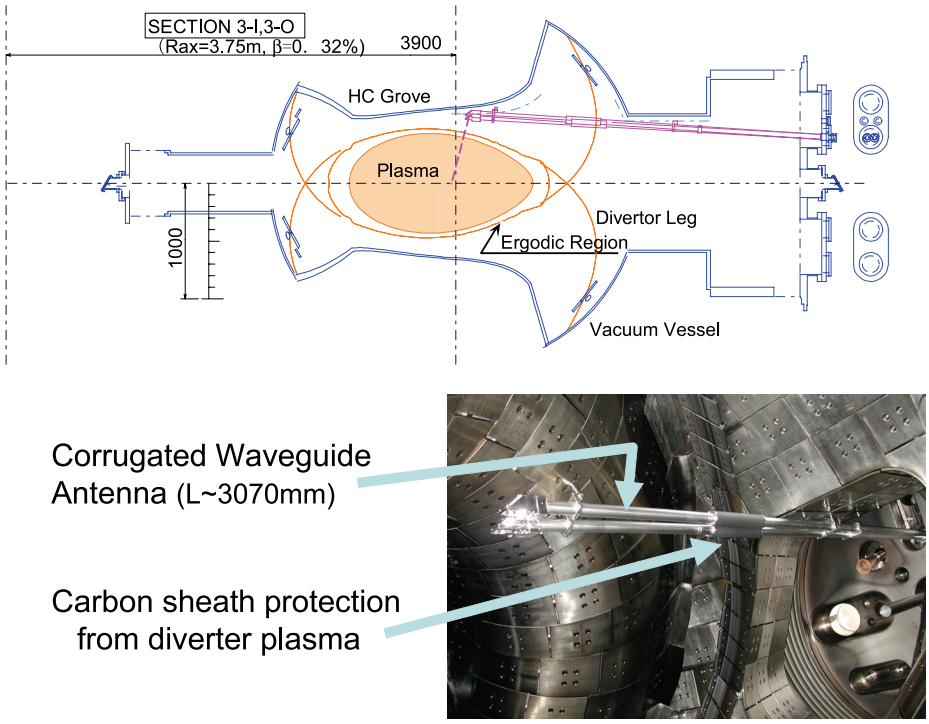

Fig. 4 Cross section of LHD and transmission line in the vacuum vessel.

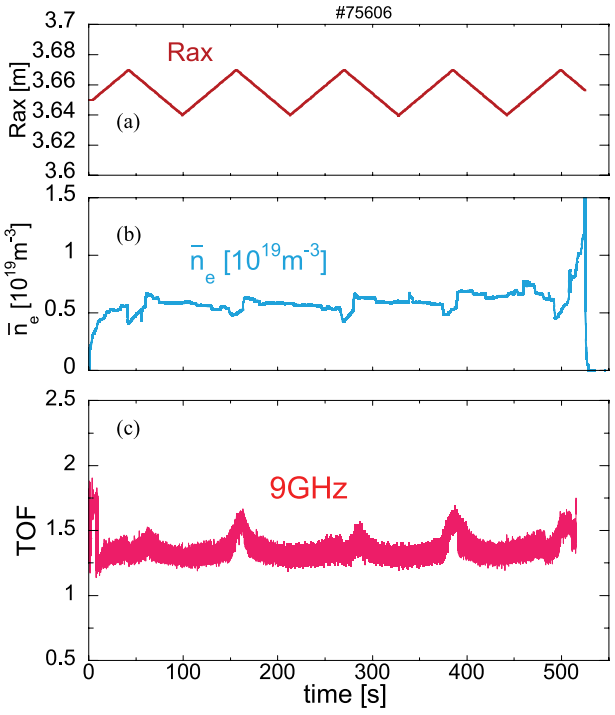

Fig. 5 Temporal evolution of (a) magnetic axis, (b) line averaged density, and (c) time of flight of reflected pulse.

plasma discharge, in which the magnetic axis is swept periodically every 108 seconds. It was observed that the electron density layer of 1×10^{18} m^{-3} also changes every 108 seconds. We can therefore successfully obtain the entire time evolution.

We now describe the optimization of the frequency bandwidth of the BPF. In TOF measurements, the spatial uncertainty of the cut-off position is related to the frequency bandwidth of the incident wave. When we use a narrower BPF, the reflected pulse originates from a smaller region around the cut-off layer, and a better spatial resolution is obtained. However, the narrower bandwidth worsens the signal-to-noise ratio (SNR). Therefore, the characteristics of several filters with bandwidths 50, 100, 200, 500, 1000, and 2000 MHz are tested experimentally. Initially, when a metal target is placed in front of the antenna in situ, a reflected wave with a central frequency of 30 GHz is measured. Figure 6 shows the detector output through the BPF for each bandwidth (ΔBW). It is observed that the pulse width in the time domain is expanded in the case of narrower BPFs. The pulse width and amplitude for each filter are plotted in Fig. 7 (a) as a function of the bandwidth. The pulse amplitude is smaller at the narrow bandwidths. Since the noise level causes the bandwidth to change little, the SNR becomes worse for narrower filters. The detector pulse width does not decrease below approximately 2 ns for bandwidths greater than 500 MHz, because of the limitation of the temporal response in our sampling oscilloscope used in this calibration test. In the LHD plasma experiment, the main noise of the reflectometer is caused by electron cyclotron emission (ECE). It is clearly observed that the noise level is reduced when the magnetic

field strength is changed such that the ECE layer does not cross the line of sight. Figure 7 (b) shows the accuracy of the TOF measurement as a function of the bandwidth of BPF. When the microwave reflects from the mirror target, the standard deviation (std) of TOF measurement is also plotted. When the bandwidth is over 200 MHz, it is seen that the uncertainty becomes sufficiently small. The minimum value is approximately 40 ps in this TOF measurement system. On the other hand, when the bandwidth is less than 100 MHz, the uncertainty increases abruptly, because the pulse width in the time domain is very large for the temporal response of the current CFD in the TOF measurement system. Therefore, a bandwidth of 500 MHz is selected for the present use.

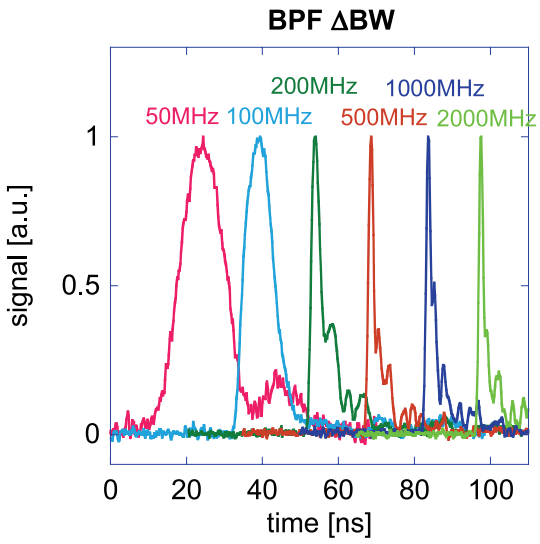

Fig. 6 Normalized waveform of detector output pulse through each BPF, the center frequency of which is 30 GHz.

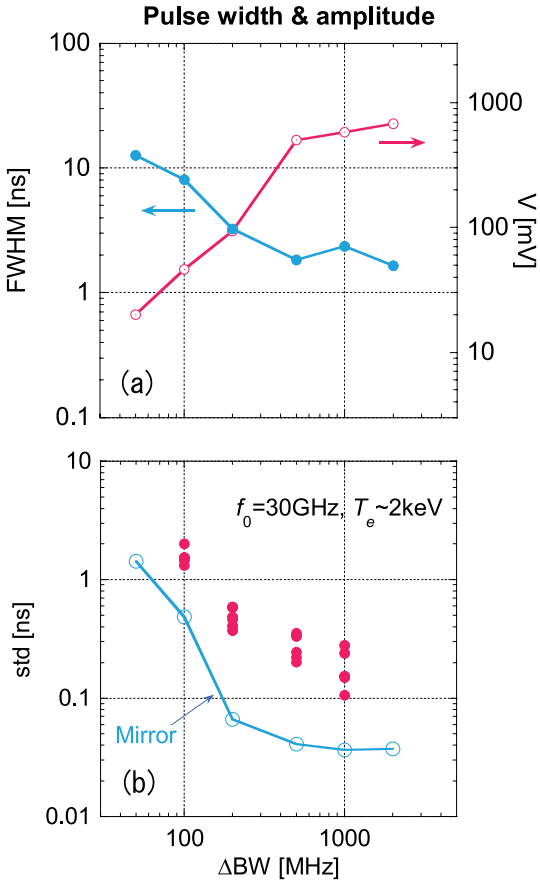

Fig. 7 (a) Pulse width and amplitude of each BPF. (b) Uncertainty of TOF measurement. Mirror reflection (open circles) and plasma experiment (closed circles).

3. The Development of a Multi-Channel and Multi-Frequency Band System

For utilizing broadband frequency components derived from an impulse, we developed several measurement techniques. Among them is a switching technique, which is applied to the multi-channel system in the Ka-band. Figure 8 (a) shows the timing diagram of the switching operation. The frequency of the local oscillator is varied from 41.5 to 42.0 GHz with a repetition rate of f_0. A SPDT switch is operated at a repetition rate of $2f_0$, with the impulse repetition rate of $4f_0$, which is generally 100 kHz. The frequency components of the detector output are then changed four times for each cycle of the oscillator frequency. For example, when the 9 and 12 GHz BPFs are paired, the measurable frequencies of the incident microwave components are 29.5, 30.0, 32.5, and 33.0 GHz. One important advantage is that there is no need for additional TOF measurement electronics, such as CFDs, TACs, or E/O converters. An example of the frequency switching operation is shown in Fig. 8 (b). When the local frequency is fixed at 42.0 GHz, the 9-GHz BPF, which has an incident frequency component of 33 GHz, is located behind a 6-way divider and the 12-GHz BPF, which has an incident frequency component of 30 GHz, is located behind another divider. When the level of the switching signal is high, only the 30-GHz signal is passed. The same discriminator then collects both the 30- and 33-GHz signals.

For the multiple-frequency band system, another required technical component is a multiplexer. To launch from the waveguide antenna into the vessel, each frequency component of three bands from the impulse source is combined to one transmission line. When we use a directional coupler for this aim, each frequency component looses more than 6 dB of power. Therefore, we designed and produced a new multiplexer. Figure 9 (a) shows the multiplexer consisting of two multi-layer mesh filters. The benefits of this multiplexer are as follows: (1) low loss, (2) free polarization requirement, (3) two-way transmission, and (4) relatively compact package. The transmissivity of each frequency component is shown in Fig. 9 (b). Here, the input microwave is launched to the correspond-

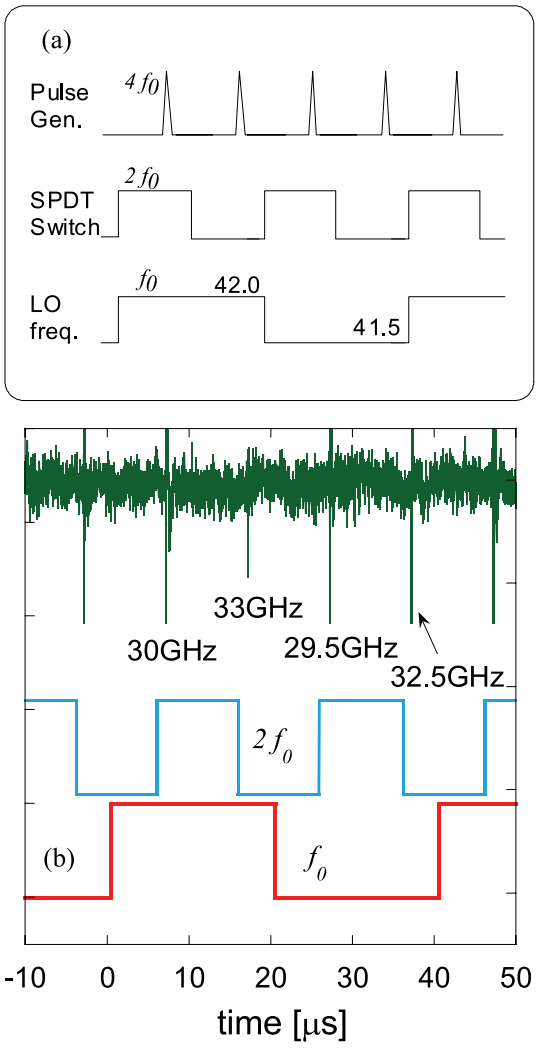

Fig. 8 (a) Timing diagram of switching operation. The frequency of the local oscillator is changed from 41.5 to 42.0 GHz with the repetition rate of f_0. The SPDT switch is operated with a $2f_0$ repetition rate. (b) Example of the frequency switching operation.

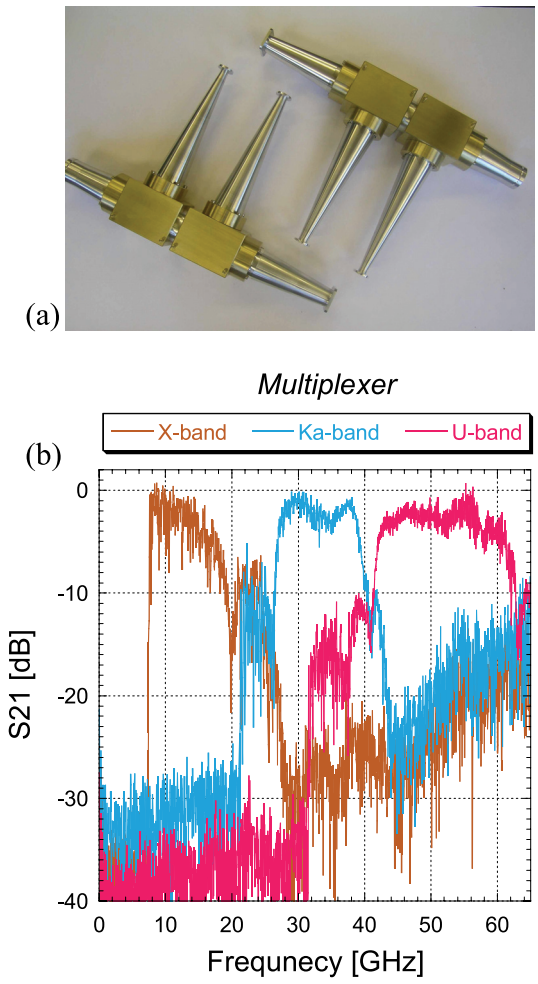

Fig. 9 (a) Picture of the multiplexer. (b) Transmissivity of each frequency component.

ing waveguide, and detected beyond the combined and divided region. Therefore, the loss from all the frequency components becomes lower than that from the previous directional coupler system. In the case of the U-band, the improvement is approximately 10 dB.

4. Density Profile Measurements

The ultrashort pulsed radar reflectometer system operates with an ordinary-mode polarization, and has 28 channels consisting of 2 channels in the X-band, 24 channels in the Ka-band and 2 channels in the U-band. The measured flight time of each frequency pulse reflected from the plasma is expressed by

$$\tau_{\mathrm{p}}(\omega_0) = \left(\frac{\mathrm{d}\phi(\omega)}{\mathrm{d}\omega}\right)_{\omega=\omega_0} = \frac{2}{c}\int_{r_{\mathrm{a}}}^{r_{\mathrm{c}}(\omega_0)} \frac{1}{\sqrt{1-\frac{\omega_{\mathrm{pe}}^2(x)}{\omega_0^2}}}\mathrm{d}x, \quad (2)$$

where r_{a} is the edge of the plasma, c is the velocity of the light, ω_0 is the probing frequency, ω_{pe} is the plasma frequency, and $r_{\mathrm{c}}(\omega_0)$ is the position where the plasma frequency equals the probing frequency. The measured delay time τ_{m} is expressed by $\tau_{\mathrm{m}} = \tau_{\mathrm{wg}} + \tau_{\mathrm{vac}} + \tau_{\mathrm{p}}$. Here, τ_{wg} is the delay time of the waveguide and τ_{vac} is the delay time in a vacuum. For determining the values of τ_{wg} and τ_{vac} at each probing frequency, we perform an in situ calibration.

An example of the temporal behaviors of the TOF of several reflected pulses is shown in Fig. 10. The experiment is conducted with a magnetic field strength of 2.75 T and a magnetic axis position of 3.60 m in the LHD. The delay time is defined by the traveling time from the plasma edge, whose position is calculated using the result of the in situ calibration and a magnetohydrodynamic (MHD) equilibrium calculation, to each cut-off layer. When the corresponding cut-off layer is generated in the plasma, each reflected wave appears in order. As the density increases, the delay time gradually decreases because the cut-off layer moves gradually towards the outside.

The result of the TOF measurement as a function of

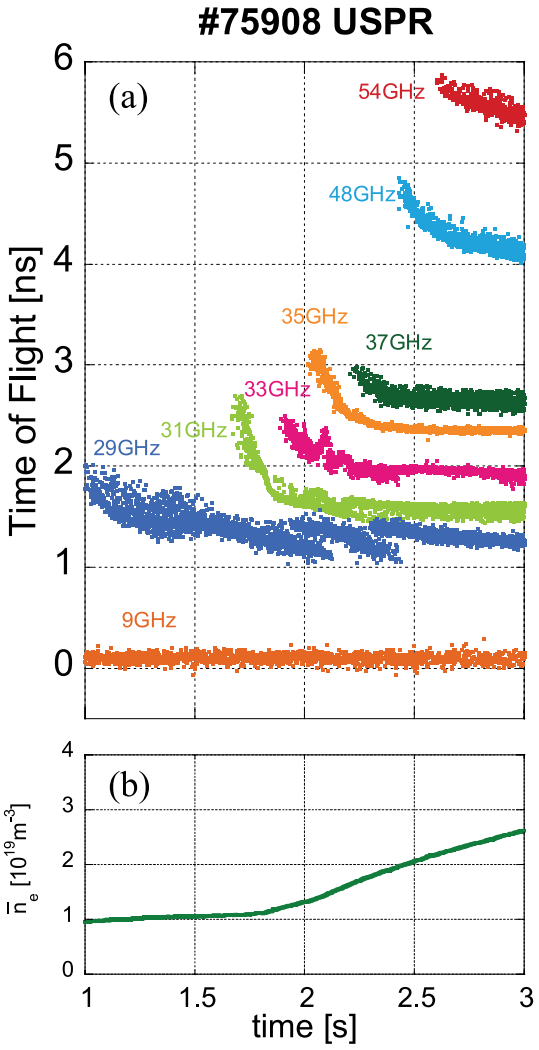

Fig. 10 Temporal evolution of (a) TOF of each reflected frequency component, and (b) averaged density.

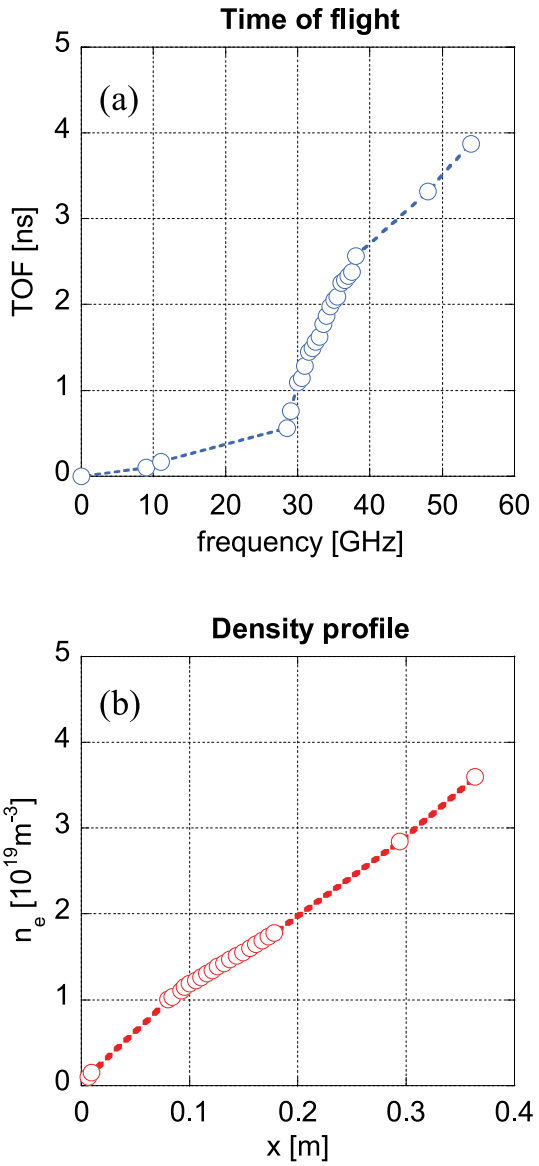

Fig. 11 (a) Profile of measured TOF of each channel as a function of the probing frequency, and (b) Reconstructed density profile.

the frequency is shown in Fig. 11 (a). Because the measured points are discrete and limited, the TOF profile has to be interpolated using a cubic spline. By Abel inversion, the position of the corresponding cut-off layer is given by

$$r_c(\omega_0) = \frac{c}{\pi}\int_0^{\omega_0} \frac{\tau(\omega)}{\sqrt{\omega_0^2-\omega^2}}\mathrm{d}\omega. \quad (3)$$

Figure 11 (b) shows the reconstructed density profile. Here the horizontal axis indicates the distance from the assumed plasma edge.

A comparison with other diagnostics such a far-infrared (FIR) laser interferometer and a Thomson scattering system is shown in Fig. 12. Here, the density profiles are plotted as a function of ρ, because each diagnostic is located in a different toroidal section and along a different line of sight in each cross section. They are almost in agreement, but some discrepancies remain at the boundary region. Therefore, we believe that more spatial channels are required for more accurate measurements particularly at the edge.

Another relevant example is presented in Fig. 13. This type of plasma discharge is the so-called ELMy H-mode-like discharge [8], with a magnetic axis position of 4.0 m and a strength of 2.475 T. It is evident that the Hα signal increases periodically. At the same time, FIR signals of the edge channels (3309 and 3399) increase, but those of core channels (3489, 3939, and 4119) are out of phase. Reflectometer signals also respond to this event. When the Hα signal increases, the cut-off layers of 36 and 33.5 GHz move towards the inside, but other channels move towards the outside. The boundary is located in the area between 33.5 and 32.5 GHz. Therefore, the edge localized mode (ELM)-like event originates in this region.

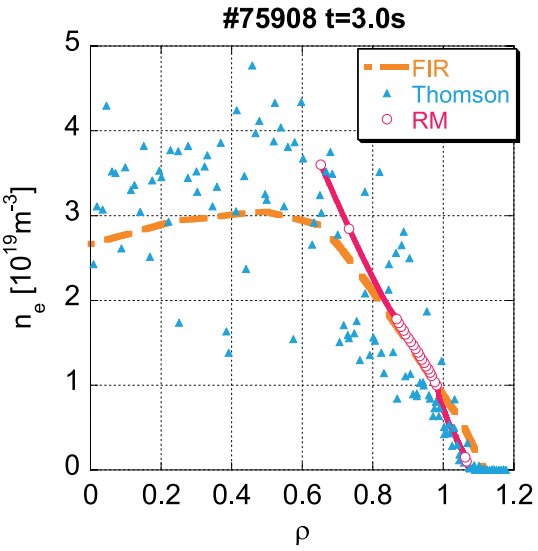

Fig. 12 Density profiles of FIR interferometer (dashed line). Thomson scattering (triangles), and reflectometer (open circles).

5. Summary

An impulse waveform voltage was utilized as a broad band frequency source for electron density profile measurements. We installed a 28 channel ultrashort pulsed radar reflectometer system in the LHD. The frequency bandwidth of the BPF was observed to be important for the accuracy of TOF measurements, the optimum bandwidth of which was obtained experimentally. For a multi-channel system, the switching technique was utilized for TOF measurements. In additional, for a multi-band system, the newly developed multiplexer exhibited good characteristics, and was shown to reduce transmission loss. Consequently, we succeeded in measuring the delay time of each probing frequency and reconstructing the electron density profile.

As a future study, an important aim would be to conduct a higher-density plasma measurement. A THz reflectometer system using a photoconductive antenna has already been planned in [9]. This is also based on a THz pulse radar technique. The pulse shape is similar to the impulse. We will try to apply this to a fusion plasma experiment in the near future.

Acknowledgements

This study was partially supported by a Grant-in-Aid from the Japan Society for the Promotion of Science to one of the authors (TT), and also by NIFS07ULHH507 from the budget Grant-in-Aid by the National Institute for Fusion Science.

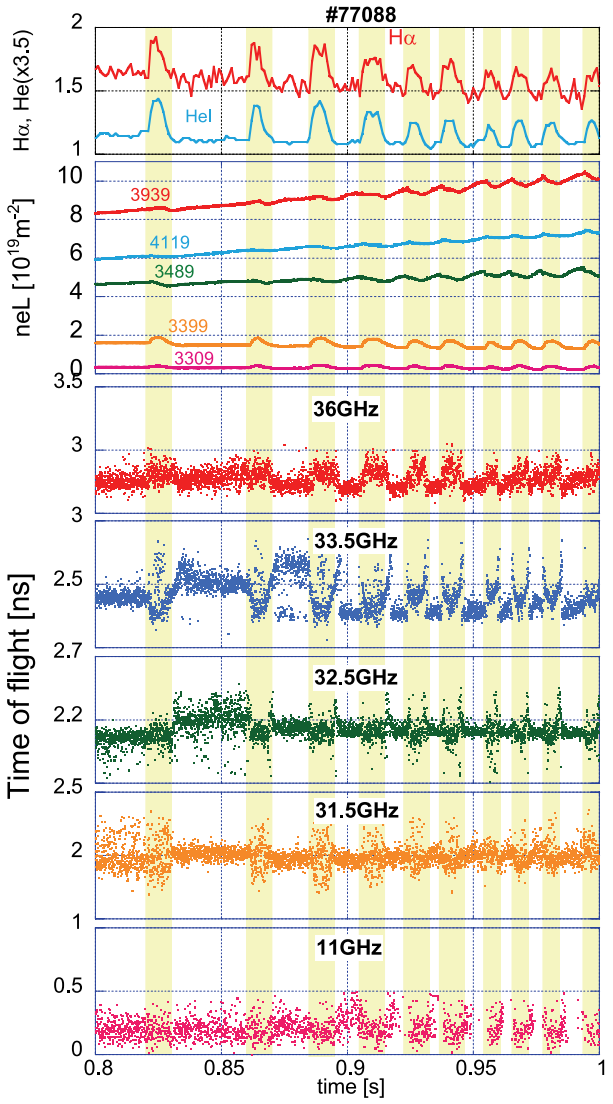

Fig. 13 Temporal evolution of Hα and HeI, the line-integrated electron density measured using a FIR interferometer, and the TOF of each reflected pulse.

[1] Y. Roh *et al.*, Rev. Sci. Instrum. **74**, 1518 (2003).
[2] C.W. Domier *et al.*, Rev. Sci. Instrum. **75**, 3868 (2004).
[3] S. Kubota *et al.*, Rev. Sci. Instrum. **70**, 1042 (1999).
[4] O. Motojima *et al.*, Nucl. Fusion **43**, 1674 (2003).
[5] T. Tokuzawa *et al.*, Nucl. Fusion **46**, S670 (2006).
[6] T. Kaneba *et al.*, J. Plasma Fusion Res. Ser. **6**, 417 (2004).
[7] H. Nakanishi *et al.*, Fusinon Eng. Des. **66-68**, 827 (2003).
[8] S. Morita *et al.*, Nucl. Fusion **47**, 1033 (2007).
[9] T. Tokuzawa *et al.*, Proc. LAPD2007 (CD-rom), Takayama, Japan (2007).